© 2022. Published by The Company of Biologists Ltd | Journal of Experimental Biology (2022) 225, jeb244245. doi:10.1242/jeb.244245

RESEARCH ARTICLE

Subsets of leg proprioceptors influence leg kinematics but not interleg coordination in *Drosophila melanogaster* walking

Alexander S. Chockley[1], Gesa F. Dinges[1,*], Giulia Di Cristina[1], Sara Ratican[2], Till Bockemühl[1,‡] and Ansgar Büschges[1,‡,§]

ABSTRACT

Legged locomotion in terrestrial animals is often essential for mating and survival, and locomotor behavior must be robust and adaptable to be successful. This adaptability is largely provided by proprioceptors monitoring positions and movements of body parts and providing feedback to other components of locomotor networks. In insects, proprioceptive chordotonal organs span joints and encode parameters of relative movement between segments. Previous studies have used whole-organ ablation, reduced preparations or broad physiological manipulations to impair the function of the femoral chordotonal organ (fCO), which monitors the femur–tibia joint, and have demonstrated its contribution to interleg coordination and walking behavior. The fCO in *Drosophila melanogaster* comprises groups of neurons that differ in their morphology and encoding properties (club, hook, claw); sub-population-level manipulations of fCO function have not been methodologically accessible. Here, we took advantage of the genetic toolkit available in *D. melanogaster* to identify sub-populations of fCO neurons and used transient optogenetic inhibition to investigate their roles in locomotor coordination. Our findings demonstrate that optogenetic inhibition of a subset of club and hook neurons replicates the effects of inhibiting the whole fCO; when inhibited alone, however, the individual subset types did not strongly affect spatial aspects of single-leg kinematics. Moreover, fCO subsets seem to play only a minor role in interleg temporal coordination. Thus, the fCO contains functionally distinct subgroups, and this functional classification may differ from those based on anatomy and encoding properties; this should be investigated in future studies of proprioceptors and their involvement in locomotor networks.

KEY WORDS: Proprioception, Locomotion, Motor network, Sensory neuron, Chordotonal organ, Optogenetics

INTRODUCTION

Proprioception provides information on the positions and movements of body parts that is crucial for the neural control loops regulating appendages, enabling precise and appropriate adjustments of posture and movements (Akay, 2020; Bässler, 1993; Burrows, 1996; Chiel et al., 2009; Strauß, 2017). Postural control, fine motor control and limb coordination are all highly dependent on specific mechanosensitive proprioceptors (Pearson, 1995; Tuthill and Wilson, 2016; Frigon et al., 2022). Proprioceptors exist throughout the animal kingdom, serving as sensors of movement, load and body position. In legged animals, proprioceptors encode state information about limbs and limb segments; these signals are received by components of motor networks to coordinate movements of body parts and ensure stable posture (Bässler, 1993; Burrows, 1996; Tuthill and Wilson, 2016; Tuthill and Azim, 2018). In insects, when leg proprioceptors, such as the chordotonal organs (CO), are mechanically disabled, interleg coordination and walking are affected, but the rather simple locomotor behavior of straight walking on a flat surface can still be performed (Usherwood et al., 1968; Cruse et al., 1984; Mendes et al., 2013, 2014).

Among the chordotonal organs, the femoral chordotonal organ (fCO; Bässler, 1965) has long been studied for its involvement in locomotor control. fCO dendrites connect to either a receptor apodeme attached to the tibia or to surrounding muscles and the distal femoral epicuticle. When the tibia rotates about the femur–tibia joint, mechanosensitive ion channels in the dendritic tips open, leading to changes in membrane potential in the sensory neurons (Field and Matheson, 1998; Cheng et al., 2010; Akitake et al., 2015). fCO neurons respond tonically to specific joint positions as well as phasically in response to movements with certain velocities and accelerations, as well as to vibration stimuli (Hofmann and Koch, 1985; Hofmann et al., 1985; Büschges, 1994; Field and Pflüger, 1989; Stein and Sauer, 1999; Mamiya et al., 2018). Individual cells can be sensitive to multiple movement parameters, and they exhibit non-linear encoding via response hysteresis (Kondoh et al., 1995; Mamiya et al., 2018). By experimentally introducing artificial changes in fCO feedback during voluntary movements in active animals, it has been demonstrated that fCO signals can markedly affect tibial movements (Weiland and Koch, 1987; Weiland et al., 1986; Zill, 1987); however, there is no information as to the putative role that fCO feedback signals may play in the generation of insect walking with respect to both intraleg and interleg coordination.

Here, we studied the role of fCO afferent information in the context of walking in the fruit fly, *Drosophila melanogaster*. The ∼150 monodendritic fCO primary sensory neurons in *D. melanogaster* can be morphologically grouped based on their stereotyped axonal projection patterns, and these patterns correlate with their response properties (Shanbhag et al., 1992; Mamiya et al., 2018). These patterns have been named *hook*, *claw* and *club* (Phillis et al., 1996). This differs from other insect species, such as the locust *Locusta migratoria*, in which morphological distinction is far less obvious (Matheson, 1992). Additionally, *Drosophila* is thus far unique in terms of the presence of a peripheral hub of synapses

[1]Department of Animal Physiology, University of Cologne, 50674 Cologne, Germany. [2]Dartmouth Geisel School of Medicine, Hanover, NH 03755, USA.
*Present address: Department of Mechanical and Aerospace Engineering, West Virginia University, Morgantown, WV 26505, USA.
‡Shared senior authorship

§Author for correspondence (ansgar.bueschges@uni-koeln.de)

A.S.C., 0000-0002-5060-6786; G.F.D., 0000-0002-1759-738X; G.D., 0000-0001-6253-4807; S.R., 0000-0002-7864-0070; A.B., 0000-0003-2123-1900

Received 8 March 2022; Accepted 20 September 2022

Journal of Experimental Biology (2022) 225, jeb244245. doi:10.1242/jeb.244245

List of abbreviations

AEP	anterior extreme position
BL	body length
ChAT	choline acetyltransferase
CO	chordotonal organs
CS	campaniform sensilla
DLC	DeepLabCut
fCO	femoral chordotonal organ
FL	front leg
GtACR1	*Guillardia theta* anion channelrhodopsin 1
HL	hind leg
ML	middle leg
PEP	posterior extreme position
tCO	tibial chordotonal organ
VNC	ventral nerve cord

between the fCO and the leg nerve; its functional role, however, has yet to be investigated (Shanbhag et al., 1992). This glomerulus, containing diverse synapses with both clear and dense-core vesicles, is likely to play a role in the preprocessing of fCO signals. Whether the different neuron types are represented differently in the glomerulus remains an open question.

Previous studies have used chronic ablation of fCO sensory neurons in reduced preparations or broad genetic manipulations to allow an assessment of the role fCO sensory feedback might play in walking behavior (Cheng et al., 2010; Mendes et al., 2013; Akitake et al., 2015). However, transient, sub-population-level manipulations of fCO function have not been possible because of methodological limitations. Here, we took advantage of the genetic toolkit available for *D. melanogaster* to perform transient, sub-population-level manipulations of the fCO in intact, freely walking animals. We identified and describe subsets of fCO neurons and their functional role in the control of walking using optogenetic inhibition. We further present the anatomy of novel *club*, *claw* and *hook* neurons in the fCO and ventral nerve cord (VNC), extending those introduced by Mamiya et al. (2018). Our results demonstrate that individual subsets of fCO neurons are vital for natural forward walking, underlining the importance of fCO feedback for the generation of walking movements.

MATERIALS AND METHODS

Experimental model and subject details

Female *Drosophila melanogaster* Meigen aged 3–8 days post-eclosion were used for all experiments. Flies were reared on a standard yeast-based medium (Backhaus et al., 1984) at 25°C on a 12 h:12 h light:dark cycle. See Table S1 for *D. melanogaster* genotypes used in this study.

VNC preparation

Flies were anesthetized on ice and briefly (<1 min) soaked in 70% ethanol to de-wax the cuticle. VNCs were dissected out in 0.1 mol l^{-1} phosphate-buffered saline (PBS) and fixed in 4% paraformaldehyde (PFA) for 30 min on ice. Following three 15 min washing steps in 0.5% Triton X-100 in 0.1 mol l^{-1} PBS (0.5% PBT), VNCs were blocked in 10% normal goat serum (blocking solution; ThermoFisher Scientific, RRID: AB_2532166) in PBT for 20 min at room temperature and incubated for 48 h at 4°C in primary antibody diluted in blocking solution [mouse anti-nc82, 1:500, Developmental Studies Hybridoma Bank (DSHB), RRID: AB_2314866; rabbit anti-GFP, 1:500, Invitrogen, RRID: AB_221569]. After three washes in PBT, they were incubated for 48 h at 4°C in secondary antibodies (goat anti-mouse AlexaFluor 633, 1:500, ThermoFisher Scientific, RRID: AB_1307538; goat anti-rabbit AlexaFluor 488, 1:500, Molecular Probes, RRID: AB_143165) followed by three washes in PBT, before being mounted in Vectashield (Vector Laboratories, RRID: AB_2336789) and covered by a coverslip.

Leg preparation

Whole flies were skewered on insect pins, briefly soaked in 70% ethanol to de-wax the cuticle, fixed in 4% PFA for 45 min on ice, and washed in 0.1 mol l^{-1} PBS (3×15 min). The tibia, tarsus and distal femur were then removed with microscissors and incubated in a blocking solution of 10% normal donkey serum (Jackson ImmunoResearch Laboratories, RRID:AB_2337258) and 5% PBT for 2 h at room temperature with nutation, then incubated with primary antibody [mouse anti-choline acetyltransferase (ChAT), 1:50, DSHB, RRID: AB_528122] in 0.5% PBT and 1% donkey serum for 72 h at 4°C. After four washes in 0.5% PBT of 1.5–2 h each at room temperature, the legs were incubated in the secondary antibody (anti-mouse AlexaFluor 488, 1:50) in 0.5% PBT and 1% normal donkey serum for 96 h at 4°C. Nuclei were then stained with DAPI (5 mg ml^{-1} in DMSO; cat. no. 6335.1, Carl Roth GmbH and Co. KG, Karlsruhe, Germany) diluted in 0.1 mol l^{-1} PBS (1:10,000) overnight at 4°C, washed 3×1 h in PBS, mounted in Vectashield and covered by a coverslip.

Fluorescence microscopy and 3D reconstruction

Confocal stacks (SP8; Leica, Wetzlar, Germany) were taken of samples with a 63× oil immersion objective (legs) or a 20× glycerol immersion objective (VNCs). Maximum intensity projections were created using Fiji (http://fiji.sc; Schindelin et al., 2012). All figures containing microscopy images were compiled using CorelDraw (X6; Corel Corporation, RRID: SCR_014235).

Confocal Z-stacks of fCO subset lines expressing nuclear-localized red fluorescent protein (RFP) were reconstructed using Amira (6.0.1; ThermoFisher Scientific, RRID:SCR_007353). First, nuclei of the RedStinger-labeled iav-GAL4 neurons were traced by hand. These outlines were then checked and corrected using the signal from DAPI-stained nuclei. The outer shell of each fCO was generated by tracing the outermost edge of the anti-ChAT signal in each slice of the Z-stack. All labels were smoothed along the three dimensions. Once smoothed, a surface mesh was generated from the data. These were then imported into Blender (2.79; Blender Foundation, RRID:SCR_008606), where they were re-meshed, smoothed and rendered. PNGs were exported from Blender. Using the final images, conservative cell body counts were completed manually.

Free-walking assay

Flies (0–2 days post-eclosion) expressing *Guillardia theta* anion channelrhodopsin GtACR1 (or wild-type>UAS-GtACR1 flies in control experiments; Mohammad et al., 2017) were transferred to vials containing food and 0.14 mmol l^{-1} all-trans retinal (R2500; Sigma-Aldrich, RRID:SCR_008988) for at least 3 days before experiments. Some flies were starved for 18–24 h prior to testing; for this, they were placed in a 2 ml plastic tube with a small piece of wet tissue. A schematic diagram of the free-walking setup is shown in Fig. 1A. It consisted of an inverted glass Petri dish that we used as a transparent arena (diameter 100 mm) held by a circular frame with a cutout below the dish. The cutout provided an unobstructed view from under the arena. To prevent flies from escaping, the arena was

Journal of Experimental Biology (2022) 225, jeb244245. doi:10.1242/jeb.244245

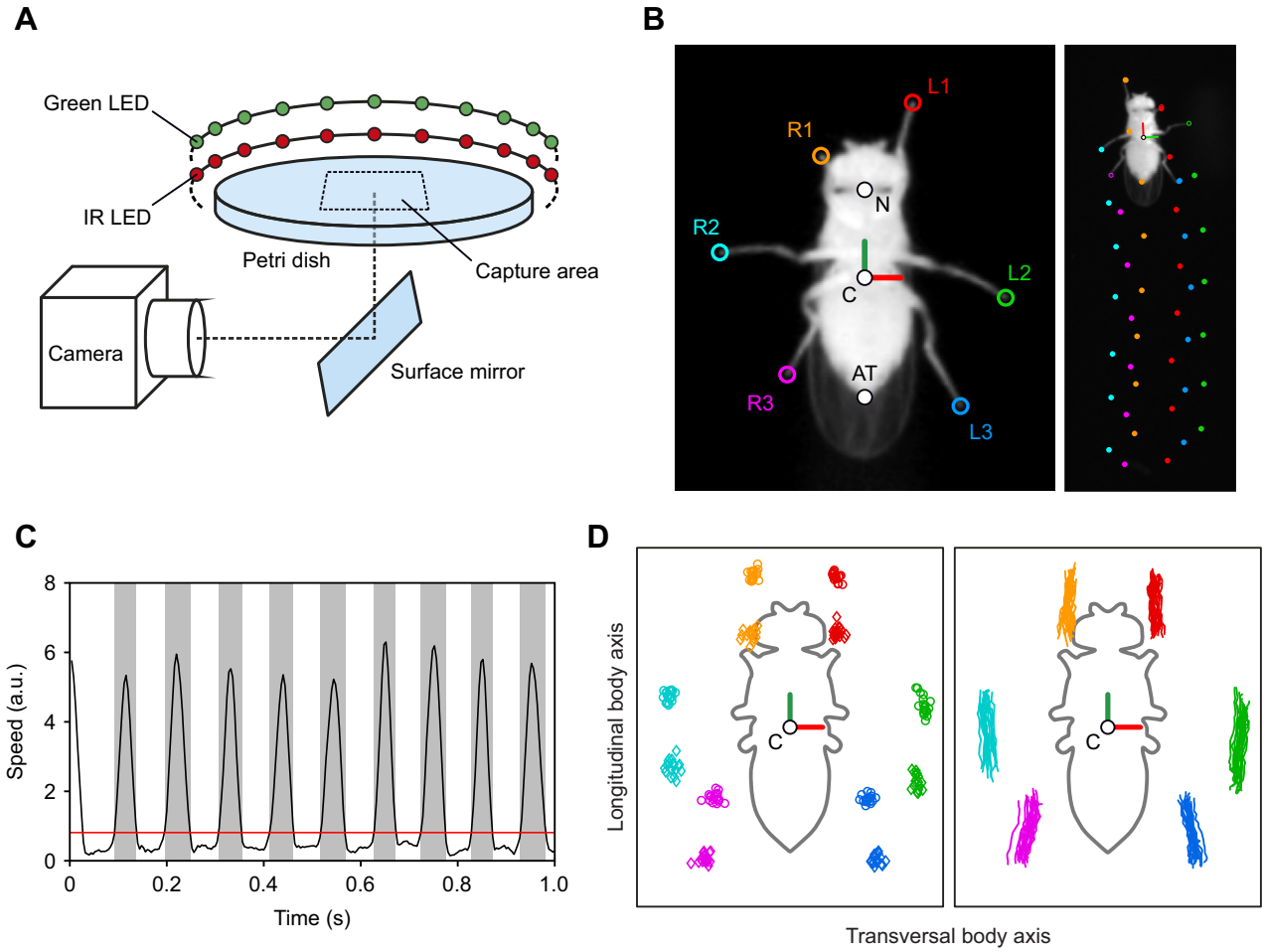

Fig. 1. Free-walking assay and analysis. (A) Schematic diagram of the setup. Flies walked on top of an inverted Petri dish while being video recorded from below via a surface mirror. Illumination was provided by an infrared (IR)-LED ring encircling the arena (red circles). An additional ring of green LEDs (green circles) above the IR-LED ring provided the illumination necessary for GtACR1 activation; entire rings are not shown for clarity. A watch glass (not shown) placed onto the Petri dish prevented flies from escaping. (B) Exemplary ventral views of a fly in the setup showing a whole trial (right) and an exemplary cropped video frame used for annotation (left). Illuminated by IR light, the fly appears bright on a black background. The neck (N) and the posterior tip of the abdomen (AT), as well as the tarsal tips of all six legs (R1–R3, L1–L3) were automatically annotated in each video frame using DeepLabCut (DLC). Note, that because of the ventral aspect, left and right body sides are flipped. A color map of these six legs is used consistently throughout the text and figures. Point C indicates the location of the center of mass and the origin of the body-centered coordinate system. (C) Detection of swing (gray areas) and stance movements. Based on the relative speed between tarsus and substrate, lift-off and touchdown times and positions were determined automatically. (D) Exemplary data of 15 individual steps of a control fly. Data are shown in a fly-centered coordinate system (point C indicates the location of the center of mass and the origin of the body-centered coordinate system; the outline of the fly's body is shown in gray). Left: individual anterior extreme positions (AEPs; circles) and posterior extreme positions (PEPs; diamonds). Right: Corresponding stance trajectories. Colors as in B. Data in C (temporal) and D (spatial) formed the basis for all kinematic analyses in this study.

covered with a watch glass that established a dome-shaped chamber, similar to an inverted FlyBowl (Simon and Dickinson, 2010). To prevent flies from walking upside down on the watch glass, we coated its inside surface with SigmaCote (cat. no. SL2; Sigma-Aldrich, RRID:SCR_008988). A surface mirror was placed below the arena at a 45 deg angle. Using this mirror and an infrared (IR)-sensitive high-speed camera (VC-2MC-M340; Vieworks, RRID: SCR_017966), we captured a bottom view of a central quadratic area on the surface of the arena of approximately 30×30 mm, with a resolution of 1000×1000 pixels, a frame rate of 250 Hz, and an exposure time of 200 µs. The arena was illuminated by a ring of 60 IR LEDs (wavelength: 870 nm) arranged concentrically around the arena; light from these LEDs was mainly emitted parallel to the surface of the arena. This resulted in a strong contrast between the background and the fly and facilitated video acquisition (see Fig. S1B). A second ring of 60 green LEDs (wavelength: 525 nm) positioned above the IR LED ring provided the light necessary to transiently activate GtACR1, thereby hyperpolarizing targeted neurons. Contrast and homogeneity were further increased by equipping the camera's lens with an IR-pass filter (cut-off frequency: 760 nm) that blocked all ambient visible light and the green light from the stimulation LEDs. IR LEDs were pulsed and synchronized to the frame acquisition of the camera (250 Hz, 200 µs acquisition time). A computer fan was used to cool the LEDs and arena from below.

Prior to an experiment, a single fly was extracted with a suction tube from its starvation or rearing vial and placed onto the arena, which was then covered with the watch glass. Flies walked spontaneously for a few hours in the arena and frequently crossed the capture area. Video data of this area were continuously recorded into a frame buffer of 5 s. Custom-written software functions evaluated the recorded frames online and determined whether a fly was present at a particular time and whether it had produced a continuous walking track that had a minimum length of 7 body

lengths (BL) with a minimum walking speed of 2 BL s^{-1}. Once the fly had produced such a track and then either stopped or left the capture area, the contents of the frame buffer were committed to storage as a trial. After this, acquisition started anew. Note that the trials acquired in this way constitute only a larger collection of raw walking data and that the specifics of minimum length and speed are not critical. Flies often produced very tortuous walking trajectories with frequent heading and speed changes. As these two parameters have very strong effects on low-level aspects of walking (such as period or interleg coordination), we narrowed down the walking episodes that were subsequently analyzed.

During an experimental session, flies either walked in darkness (control condition) or under green-light illumination (inhibited condition). These two conditions were alternated in the following way: after a fly produced a valid control trial, the green light was switched on for 60 s, during which the recording system was primed to record a trial. Once this happened, the light was switched off again and the system was be primed for the next valid control trial, and so on. If the fly failed to produce a valid trial during the on-time of 60 s, the recording system would be paused and the light would be switched off again for 60 s. We used this cooldown to prevent extended periods of neuronal inhibition and temperature increases from the green LEDs. After the cooldown period, the green light was switched on again and the system was primed for the acquisition of a valid trial (again for 60 s). Switches from green light to cooldown were repeated until the fly produced a valid trial during green light illumination, after which the system was primed for the next valid control trial. The green LEDs were controlled using a digital I/O device (USB-6501; National Instruments Corporation, Austin, TX, USA). Automatic video acquisition, online evaluation and light control during experiments were implemented in MATLAB (2014b; RRID:SCR_001622).

Free-walking data selection and annotation

As mentioned before, previous studies, particularly in *D. melanogaster*, have shown that many parameters of walking in insects are strongly dependent on walking speed (Strauß and Heisenberg, 1990; Wosnitza et al., 2013; Mendes et al., 2013). Therefore, after automatic trial acquisition, but prior to any further data analysis, we manually selected walking episodes from within complete trials that had low intra-trial variability in walking speed, in which flies walked in a straight line, and that contained at least five consecutive steps. Furthermore, to exclude random walking speed-dependent differences between conditions, these walking episodes were further selected so that the two conditions (control and inhibited) had similar speeds (within 6 mm s^{-1} of each other). These pre-selected episodes served as the basis for further analysis of low-level, walking-related kinematic and coordination parameters.

First, the position of the fly throughout an episode was determined automatically. Each video frame was converted into a binary image (black background, bright fly), in which the fly was detected as the largest bright area following a simple threshold operation. Walking speed was calculated as changes of the center of mass of this area over time. We then used this positional information to crop the fly from the original 1000×1000 pixel video. These smaller and fly-centered video sequences were used for annotation of eight different body parts in every video frame: the tarsal tips of all six legs, the neck and the posterior tip of the abdomen (Fig. 1B). This step of the annotation was done automatically in DeepLabCut (DLC; Mathis et al., 2018); we trained and evaluated DLC with a dataset of 1000 manually annotated video frames (10 flies, 100 frames each), that were similar to the ones we recorded during the experiments described herein but were not part of the present study. One half (10 flies, 50 frames each) of this set was used for training, and the other half was used to evaluate its performance. Performance of DLC was generally good; however, to ensure high-quality annotations, we inspected the results visually and, if necessary, manually corrected mis-annotations.

Free-walking kinematic analysis

To determine the times of lift-off and touch-down for each leg in a walking sequence, the DLC-determined positions of the tarsal tips were transformed into a world-centered coordinate system. In this coordinate system, a leg tip is stationary (i.e. has a speed of close to 0 mm s^{-1}) when the leg is touched down (here, defined as the stance movement) and moves markedly with respect to the ground when it is lifted off (here, defined as the swing movement). These measures and an empirically determined threshold were used to distinguish swing and stance movements (Fig. 1C). Transitions between these two were defined as touch-down and lift-off events, and the positions of the tarsal tip at these times were defined as the anterior and posterior extreme positions (AEP and PEP) in fly-centered coordinates (Fig. 1D, left). A single step of a particular leg was then defined as its movement between two subsequent PEPs; its period was defined as the time difference between two subsequent PEPs. Swing movement and duration were defined as the movement and the time difference, respectively, between a PEP and the subsequent AEP; stance movement and duration were defined as the movement and the time difference, respectively, between an AEP and the subsequent PEP. A stance trajectory was defined as the complete path of a tarsal tip in fly-centered coordinates between an AEP and the subsequent PEP (Fig. 1D, right). Step amplitude was defined as the distance between a PEP and the subsequent AEP. Average AEPs and PEPs were defined as the arithmetic mean of all AEP and PEP position vectors, respectively; the standard deviation of these positions was estimated as a bivariate distribution. To increase the compactness of the data, and because flies are bilaterally symmetric, we pooled AEPs and PEPs for front, middle and hind legs, respectively. Individual shifts in extreme positions during inhibition were calculated as vectors between the mean AEPs/PEPs in the control condition and their respective individual AEPs/PEPs during the inhibited condition; these can be described with anatomical directions (posterior, anterior, medial and lateral). Stance trajectories were averaged by first resampling all n trajectories to 100 equidistant 2D positions (100×2 data points) and then calculating the arithmetic mean for each set of 100×2×n data points.

Free-walking phase analysis

Phase relationships (i.e. phase differences) were calculated for all ipsilaterally or contralaterally adjacent leg pairs. This resulted in seven phase relationships: three contralateral leg pairs (front, middle and hind legs) and four ipsilateral leg pairs (left and right hind and middle legs, left and right middle and front legs). A reference leg was selected for each leg pair. For contralateral phase relationships, this was always the left leg; for ipsilateral phase relationships, this was the posterior leg. For each complete step of the reference leg (PEP to PEP) we calculated its instantaneous phase as a value that linearly increased from 0 to 1 during the step. We then calculated the phase relationship between the two legs as the phase value at the times of PEPs in the non-reference leg; this was equivalent to the phase difference between these legs. A value of 0 indicated synchronous lift off, while a value of 0.5 indicated an anti-phase relationship. Similar to AEPs and PEPs, we pooled phases between hind and middle legs and middle and front legs, resulting in five

phase relationships, two ipsilateral and three contralateral. The phase between two legs is given as, for instance, HL>ML, where a hind leg (HL) is the reference leg and a middle leg (ML) is the non-reference leg.

Aside from DLC-based functions (for details, see Mathis et al., 2018), all annotations, calculations and statistics for the kinematic as well as the phase analysis were carried out with custom-written functions in MATLAB 2018b (RRID:SCR_001622; see also 'Statistical analyses', below) and the MATLAB CircStat toolbox (Berens, 2009).

Statistical analyses

To facilitate comparison between the control and inhibited conditions, we normalized all individual step periods, swing durations, stance durations and stance amplitudes to the arithmetic mean of the control condition. Flies differ naturally with regard to these parameters, and normalization allows for direct comparison between flies and pooling of all data.

For statistical tests concerning swing, stance and step duration, we used the non-parametric two-sided Wilcoxon signed-rank test. For statistical tests concerning phase relationships, we used a non-parametric variant of the Kruskal–Wallis test for circular data as implemented in the circular statistics toolbox for MATLAB (function *circ_cmtest.m*; Berens, 2009). It should be noted that, because of the extensive dataset and the correspondingly high sample size, many of the tested differences are highly significant. We therefore also report effect sizes (which in many instances are still small, even though statistically significant) and restrict the results and discussion to large effect sizes.

RESULTS

The fCO consists of multiple anatomical subpopulations

To tease apart the role of the fCO (Fig. 2A) and subsets of its neurons in leg movements and coordination during walking, we first identified several Gal4 driver lines (Jenett et al., 2012) labeling subpopulations of fCO neurons via a manual search of the FlyLight database (HHMI Janelia Research Campus, http://flweb.janelia.org/cgi-bin/flew.cgi) and the relevant literature. We identified four driver lines of particular interest using the CO driver line *iav*-Gal4 as a reference (Fig. 2B). These labeled different subsets of fCO neurons (club, hook and claw neurons; Mamiya et al., 2018), allowing a differential analysis of the contributions of fCO neuron subtypes to kinematics and coordination during walking. We identified driver lines labeling club and hook neurons (R27E02-Gal4, ∼60 cell bodies; Fig. 2C), claw neurons (R55B03-Gal4, ∼6 cell bodies; Fig. 2D), club neurons (R46H11-Gal4, ∼30 cell bodies; Fig. 2E) and hook neurons (R86D09-Gal4, ∼60 cell bodies; Fig. 2F). 3D surface reconstructions based on driver line-expressed, nuclear-localized RFP (UAS-RedStinger) as well as anti-ChAT antibody labeling and DAPI staining to label mechanosensitive neurons and all nuclei, respectively, showed that these driver lines label varying numbers of cells within the fCO itself (Fig. 2C–F). As a reference, we used *iav*-Gal4, a driver line that labels the majority of fCO neurons (Fig. 2B; Tsubouchi et al., 2017).

The primary sensory neurons labeled by *iav*-Gal4 and the club/hook line project both intersegmentally and locally (Fig. 2B,C); these projection patterns can be disentangled when inspecting the expression patterns of the fCO subset lines used herein (Fig. 2D–F). Club neurons exhibit direct inter-ganglionic connectivity (between thoracic ganglia T1–T2 and T2–T3; Fig. 2E). Hook neurons show inter-hemiganglionic connectivity (left–right; Fig. 2F). Claw neurons are unique among the three subset driver lines in that they only contain local VNC projections from each leg nerve (Fig. 2D).

These subset lines labeled different numbers of cell bodies in the fCO, but no clear spatial clustering could be seen in our analysis (Fig. 2B–F). Further, ascending projections going directly to the brain (anterior ventrolateral protocerebrum) can be seen in *iav*-Gal4 (Tsubouchi et al., 2017) and in the club/hook line (Fig. 2B,C), but ascending neurons were not labeled by the other subset lines shown here (Fig. 2D–F). This indicates that some, but not all, club or hook neurons project to the brain. Particular aspects of the signals from these neurons could be important for central motor control; alternatively, this could represent a simple 'high-level' monitoring of the states of effectors. High-level monitoring, in this sense, would entail more general information that is integrated over several steps instead of the specifics of individual low-level parameters, such as the placement of AEPs and PEPs. High-level parameters based on fCO information that might be extracted in this way could include the current walking speed, based on stance duration and speed, or heading information, based on their differential magnitudes on ipsilateral body sides. This information, in turn, could be used to inform higher-level centers in the brain that control these parameters.

Furthermore, it is important to note that these driver lines did not exclusively label neurons in the fCO; some labeling was seen in the Johnston's organ of the antenna as well as chordotonal organs associated with the coxa (data not shown). Furthermore, the club/hook line labeled some campaniform sensilla (CS) of the trochanter, and the hook line labeled neurons in the tibial chordotonal organ. The club/hook line also labeled CS of the femoral and trochanteral fields (FeF and TrF; Dinges et al., 2021). The design of the experiments herein was intended to exclude potential effects of these extra-fCO neurons by ensuring that the expression patterns of these driver lines mainly intersected in the fCO. Further, to exclude influences of CS, *iav*-Gal4 served as a baseline for the influence of the fCO on walking kinematics.

Aside from potential connections between fCO neurons in the VNC, many presynapses from fCO neurons are present within the fCO itself as well as in the glomerulus, a synaptically dense structure through which fCO axons pass just before joining the leg nerve (Shanbhag et al., 1992). Synaptotagmin-bound green fluorescent protein (GFP) expression in *iav*-Gal4 and our subset driver lines showed presynapses within the fCO in all lines tested (Fig. S1A–E). Moreover, *iav*-Gal4 and R27E02-Gal4 showed labeling in the glomerulus (Fig. S1A,B, white arrows). Intra-fCO connections seem, therefore, to be a general feature among these neurons, while glomerulus-associated connections seem to be restricted to certain neurons.

Inhibition of fCO and subsets affects leg kinematics and spatial coordination in walking

To investigate the involvement of neuronal subsets in the fCO in walking behavior, we drove expression of an anion channel rhodopsin (GtACR1; Govorunova et al., 2015, Mohammad et al., 2017) in fCO neurons of freely walking flies. This enabled us to inhibit specific fCO subpopulations during natural locomotion. This use of transient, light-based neuronal inhibition allowed us to use each fly as its own control to highlight the effects of fCO inhibition over the natural inter-individual variability seen in walking (Delcomyn and Cocatre-Zilgien, 1988). Video trials of straight walking were captured under either IR illumination only (control condition) or green LED illumination (525 nm, inhibited condition; IR illumination also used here) to activate GtACR1 (Fig. 1A). Videos were cropped, and the positions of the tarsal tips were

Journal of Experimental Biology (2022) 225, jeb244245. doi:10.1242/jeb.244245

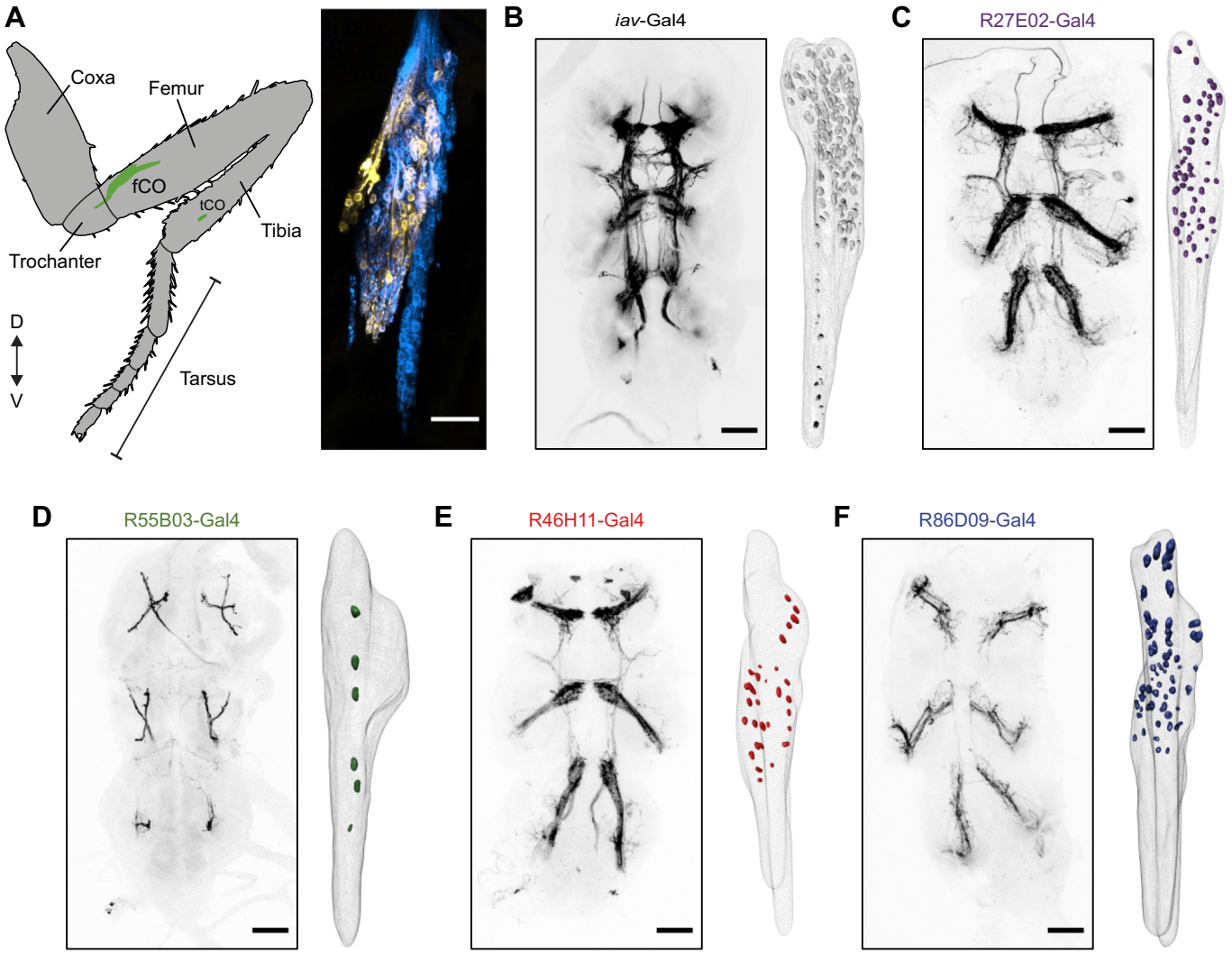

Fig. 2. Anatomy of **femoral chordotonal organ (fCO)** labeling and **ventral nerve cord (**VNC**)** projection patterns of fCO Gal4 driver lines. (A) Left: schematic diagram of a *Drosophila melanogaster* leg showing the femoral (fCO) and tibial chordotonal organs (tCO). D, dorsal; V, ventral. Right: depth color-coded confocal stack of fCO in *iav*-LexA expressing myrGFP. (B–F) Z-projections of confocal stacks of VNCs of flies expressing fCO-Gal4>UAS-mcd8::GFP show the projection patterns of the entire fCO (B) as well as fCO subsets (C–F). The colors of the panel titles are used throughout the text and figures to identify a specific Gal4 line. 3D reconstructions (on the right in each panel) show nuclei of labeled cells (UAS-RedStinger, DAPI staining) within the fCO (anti-ChAT immunolabeling), shown proximal (top) to distal (bottom). For clarity, images of confocal stacks have been converted to grayscale, with the GFP signal indicated by darker shades. VNC scale bars: 50 µm.

determined using DLC (Fig. S1B; Mathis et al., 2018). Touch-down and lift-off events were automatically detected (Fig. 1C), allowing us to extract parameters related to leg kinematics and coordination (Fig. 1D). Parameters reflecting spatial control and coordination, such as the AEP and PEP of each step, stance amplitude (distance between AEP and PEP; Fig. 1D) as well as stance, swing and step duration, were extracted from the tarsus tracking data. Control flies (Berlin-K>UAS-GtACR1) fed all-trans retinal were remarkably consistent under IR and green light illumination but exhibited interindividual variability, as was expected (Figs S2 and S3A); we only detected a slight increase in the phase relationships between ML and HL (but see Discussion).

As a first step towards understanding the functional role of the fCO in locomotion, we inhibited the majority of fCO neurons using the broad *iav*-Gal4 driver line (Tsubouchi et al., 2017). Flies were still able to walk, albeit with altered kinematics and coordination, suggesting that the fCO contributes to motor output during walking (Fig. 3). A similar finding has been reported by Mendes et al. (2013) using more permanent neuronal manipulations during walking. However, the temporally precise, transient manipulations used in the present study led to pronounced deficiencies mainly in kinematics and, to a small extent, in coordination. This was reflected in an increase in stance amplitude (Fig. 3A,C, +18–30%), which was most pronounced in the front legs (+30%). In general, these increases in stance amplitude seem to be mainly associated with posterior shifts in the PEP in all affected legs (Fig. 3Aii,B). Moreover, swing, stance and step duration were also increased in all legs (Fig. 3C). Swing duration was increased less in front legs (FL; +5.7%) than in HL (+14%), stance duration was increased less in ML (+7%) and in FL (+19%) and HL (+14%), and the other parameters changed similarly for all legs. These retardations in stepping frequency, reflected by increased step duration, were accompanied by increases in step amplitude (+16–30%). As walking speeds were matched between control and inhibited trials, these results indicate that the rate of movements during stance was unaffected and only the frequency changed.

Journal of Experimental Biology (2022) 225, jeb244245. doi:10.1242/jeb.244245

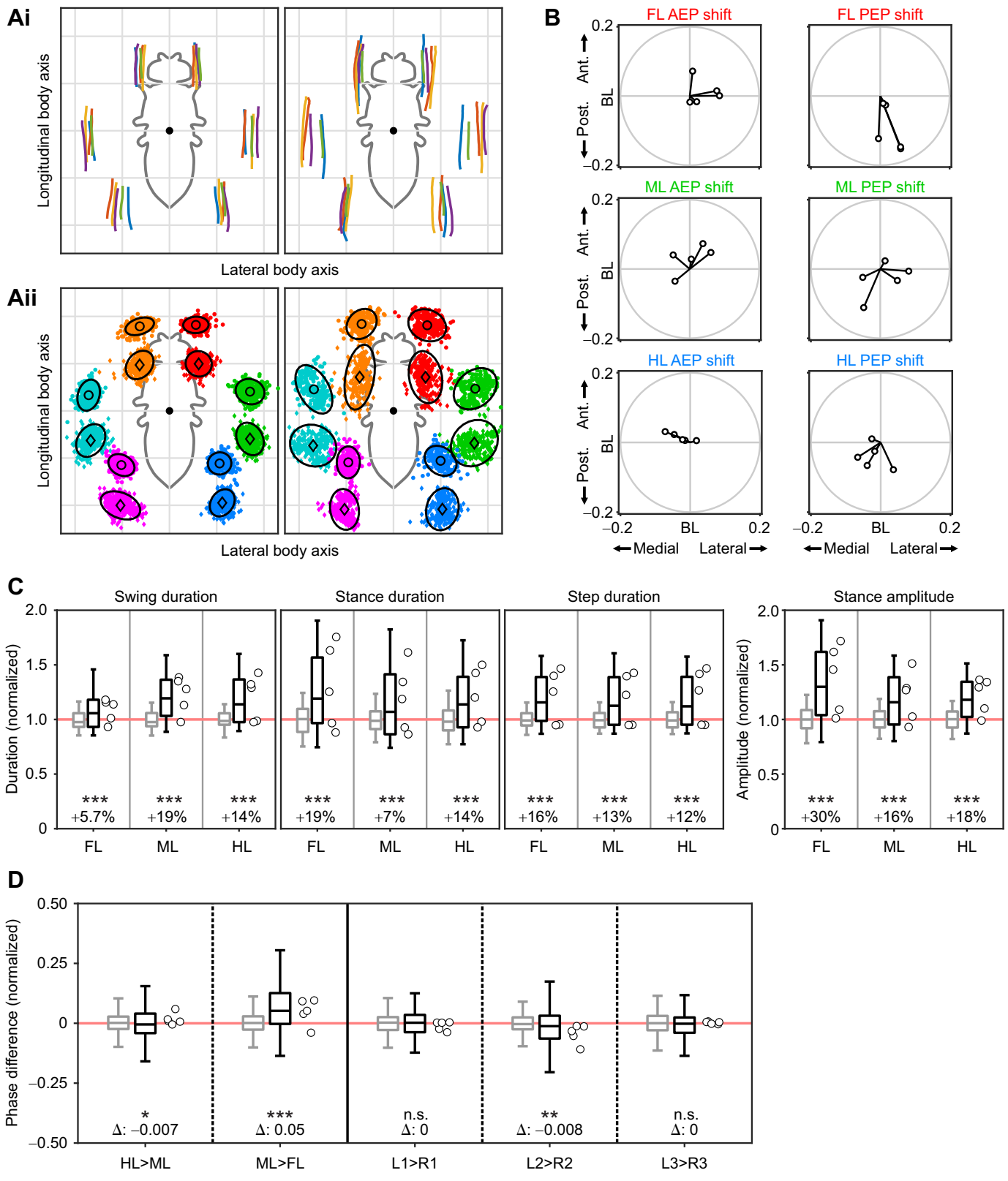

Fig. 3. See next page for legend.

Inhibition of club/hook neurons (R27E02-Gal4) resulted in elongation of stance trajectories similar to that seen in *iav*-Gal4 (Fig. 4Ai,Aii). Interestingly, although this line labeled fewer neurons, these effects were generally equally strong, if not stronger, compared with the broader *iav*-Gal4 line. Swing and stance duration changed in all legs, with some differences between leg types (Fig. 4C). Swing duration changed most in HL (+29%) and least in FL (−0.68%), whereas stance duration increased most in FL (+50%) and least in HL (+24%). Stance amplitude was increased in a pattern similar to stance duration (+25−79%). Similar to the

Journal of Experimental Biology (2022) 225, jeb244245. doi:10.1242/jeb.244245

Fig. 3. Kinematic parameters and temporal coordination of free-walking inhibition of fCO neurons in *iav*-Gal4. (Ai) Average stance trajectories for all flies (*N*=5, each fly is a different color), shown in fly-centered coordinate space for the control (left) and inhibited condition (right), as well as (Aii) the corresponding distribution of AEPs (circles) and PEPs (diamonds) with their mean positions (black circles and diamonds) and 95% percentiles (black ellipses) in the control (left) and inhibited condition (right). Individual colors in A indicate specific legs (for color map, see Fig. 1B). The minimum number of steps (*n*) per leg in Aii is 388 (control) and 238 (inhibition). For reference, the outline of the fly's body is shown in gray. (B) Average AEP and PEP shifts for each fly (*N*=5) for front, middle and hind legs (FL, ML, HL), respectively. For clarity, data from the right body side (see also Aii) have been mirrored to the left side and combined with these data. Each vector denotes one fly and indicates the average shift of AEPs and PEPs, respectively, in the inhibited condition compared with their respective mean positions in the control condition. BL, body length. (C) Kinematic parameters calculated for complete steps for control (gray) and inhibited (black) conditions. All data shown here have been normalized on a per fly basis to their mean values in the control condition (indicated as 1, light red reference line). Box plots (whiskers indicate 1% and 99% percentiles) are combined normalized data for all flies; circles indicate medians for individual flies (*N*=5). Combined data in the inhibited condition were tested against a median of 1 with a two-sided Wilcoxon signed rank test. Significance levels of these tests are given as non-significant (n.s.), *$P\leq0.05$, **$P\leq0.01$ and ***$P\leq0.001$. Effect sizes are given as the difference between the median in the inhibited condition and 1 (normalized control condition). The minimum number of steps (*n*) per leg is 750 (control) and 458 (inhibition). (D) Phase relationships between ipsilateral (HL>ML and ML>FL) and contralateral leg pairs [left front leg (L1)>right front leg (R1), left middle leg (L2)>right middle leg (R2) and left hind leg (L3)>right hind leg (R3)] for control (gray) and inhibited (black) conditions. Note, that data for ipsilateral legs have been pooled. Specifics of box plots and circles as in C. Combined data in the inhibited condition were tested against the data in the control condition with a non-parametric variant of the Kruskal–Wallis test for circular data. Significance levels and annotation as in C. Effect sizes are given as absolute differences between the median of the inhibited condition and 0. Absolute effect sizes smaller than 0.005 have been rounded to 0. *n*=374 (control) and 226 (inhibition).

results for *iav*-Gal4, these increases in stance amplitude seem to be mainly associated with posterior shifts in the PEPs in all affected legs (Fig. 4Aii,B); however, smaller anterior shifts in AEPs are also visible. Step duration in this line was increased somewhat equally in all legs (+26−27%). Flies still walked in a coordinated manner, but it is clear that inhibition of these fCO neurons affected flexion movements. In the anteriorly oriented FL, flexion is associated with stance movement as femur–tibia joint flexion pulls the fly forward. In the posteriorly oriented HL, flexion is associated with swing movements; here, the fly flexes the femur–tibia joint to move the tarsus in the air from the PEP to the AEP. In the ML, flexion is used to a smaller extent in both stance and swing movements, and both of these movements seem to be affected.

Surprisingly, inhibition of club, hook and claw neuron types individually did not ostensibly affect stance trajectories or kinematic parameters (Figs 5 and 6). This coincides with the apparent absence of synapses from these neurons in the glomerulus (see Fig. S1C,D), but any causal relationships here must be investigated in detail.

fCO inhibition only mildly affects interleg coordination in walking

Temporal interleg coordination is determined by the phase relationships between adjacent leg pairs (ipsilateral and contralateral). We defined a complete step cycle in a leg as the movement between two consecutive lift-offs (PEPs) and normalized that time span to 1, the reference phase. To then determine the phase relationship between two legs, we expressed the PEP of a dependent leg in terms of normalized phase of the reference leg; for instance, HL>ML describes the phase relationship of a middle leg in reference to its ipsilateral right hind leg. Thus, a phase relationship of 0 indicates stepping in unison (i.e. lift-offs occur at the same time). A value of 0.5 means anti-phase alternation. We then defined the mean phase relationship during the control condition as a reference phase of 0 and expressed the changes during inhibition as the difference from the reference phase. Positive values of this measure thus indicate a later PEP in the dependent leg during inhibition.

Demonstrating the relationship between the fCO and coordination, *iav*-Gal4-mediated fCO inhibition caused mild phase delays (∼5%) in swing onset between ipsilateral front and middle legs (ML>FL; Fig. 3D; for absolute phase relationships, see Fig. S3). Interestingly, effects on coordination were not seen between ipsilateral hind and middle legs, suggesting that changes in the movement of the front legs, more specifically a delayed lift-off, are responsible for this effect. In the data from *iav*-Gal4, this delay might also be reflected in the front leg stance amplitudes being the most strongly elongated (Fig. 3Ai,C). The phase relationships between hind and middle legs, however, were unchanged (HL>ML, Fig. 3D), while the stance amplitudes in these legs were also larger. This suggests uniform shifts in the absolute phases in these legs, thus negating any shifts in their relative temporal coordination. This was also seen for hook, claw and club subset neurons (Fig. 6). It should be noted that this pattern was also seen in control flies (Fig. S2) and it was not seen in the club/hook line (Fig. 3C). Compared with the effects found for the spatial parameters, these effects are small, indicating a lesser role of the fCO for temporal coordination.

DISCUSSION

fCO neurons are mainly involved in spatial aspects of leg kinematics

Signals from the fCO are crucial for the control of the femur–tibia joint during resistance reflexes and active movements (Bässler, 1967; Zill, 1987; Weiland and Koch, 1987), and interrupting synaptic transmission from leg COs broadly affects walking kinematics (Mendes et al., 2013). Coupled with the present data, it becomes clear that, during walking, fCO neurons are mainly involved in leg kinematics and postural control. When inhibiting the majority of fCO neurons using *iav*-Gal4, we found that tarsal touch-down and lift-off positions were shifted and that kinematic parameters were affected similarly in all leg types. Coordination (i.e. temporal relationships) between adjacent leg pairs, however, was only mildly affected (Fig. 3D). This was also true for the neurons labeled by the club/hook driver line (R27E02-Gal4; Fig. 4), but not for club, claw or hook neurons when inhibited alone (Figs 5 and 6). As inhibition of the entire fCO and a large group of club/hook neurons (R27E02-Gal4) both increased stance amplitude (*iav*-Gal4: +16−30%; R27E02-Gal4: +25−79%), it is clear that these neurons are important for the determination of AEP and PEP as well as the stepping frequency during walking. Given its nature as a sensory structure measuring angular positions (and derived parameters such as angular velocity and acceleration), the fCO's output should be more important for the control of tarsal placement or stance speed than for the timing of transitions between swing and stance. These last temporal aspects, which are also crucially influenced by the current state of other legs and not only intraleg information, likely rely more on the CS system (Dinges et al., 2021), as these sensory structures are typically more phasically active,

Journal of Experimental Biology (2022) 225, jeb244245. doi:10.1242/jeb.244245

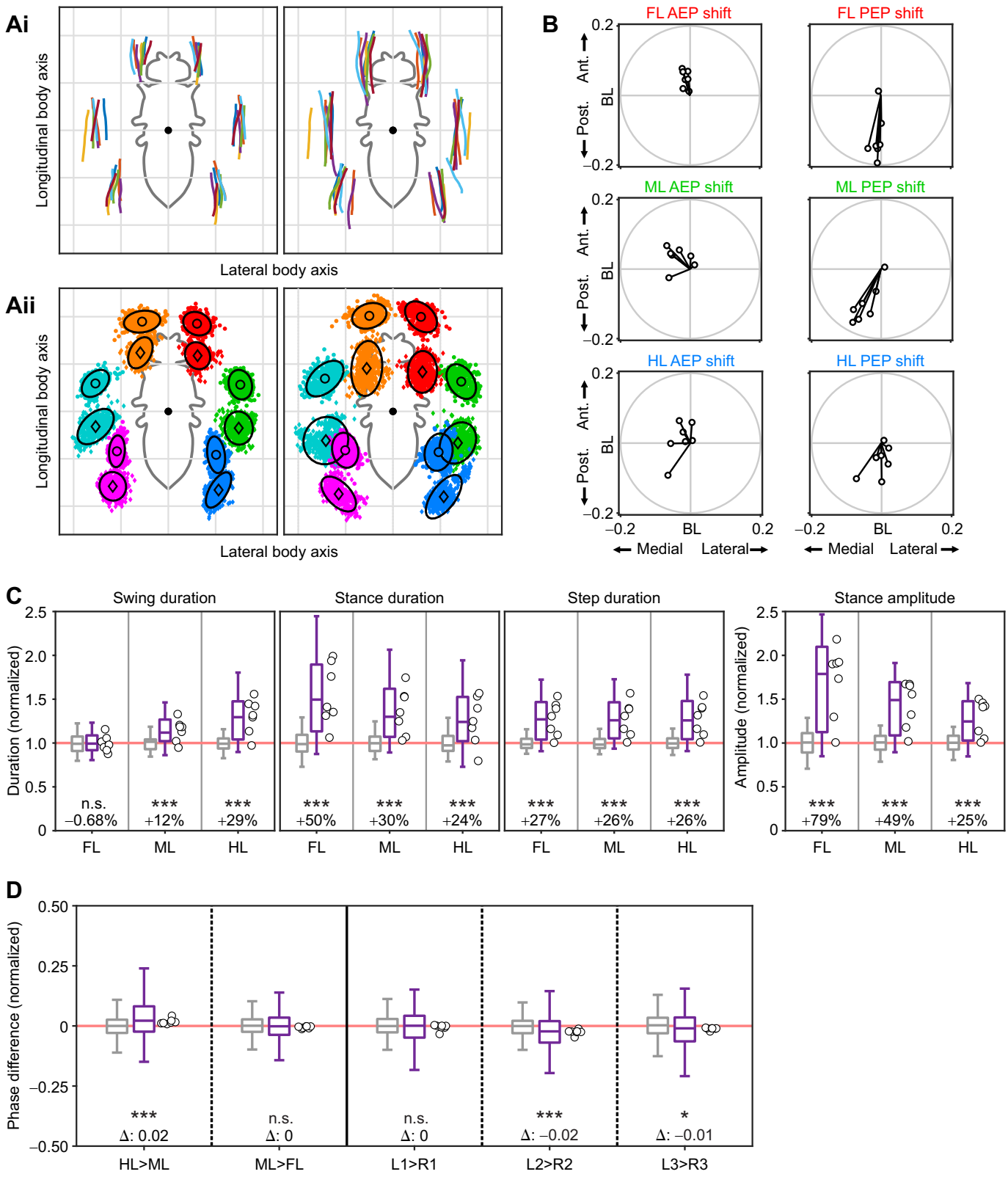

Fig. 4. Kinematic parameters and temporal coordination of free-walking inhibition of club and hook neurons in R27E02-Gal4 line. For a detailed description, see Fig. 3 legend. Note, that in order to accommodate the larger effect sizes, the scale of the *y*-axis was changed as compared with all other comparable plots. (Ai) Number of individual flies (*N*) is 7; each fly is a different color. (Aii) The minimum number of steps (*n*) per leg is 540 (control) and 528 (inhibition). (B) *N*=7. (C) *N*=7; *n*=1046 (control) and 1023 (inhibition). (D) *N*=7; *n*=521 (control) and 509 (inhibition). In B and D, the color associated with inhibition data has been set to dark magenta (R27E02-Gal4; see also Fig. 2).

Journal of Experimental Biology (2022) 225, jeb244245. doi:10.1242/jeb.244245

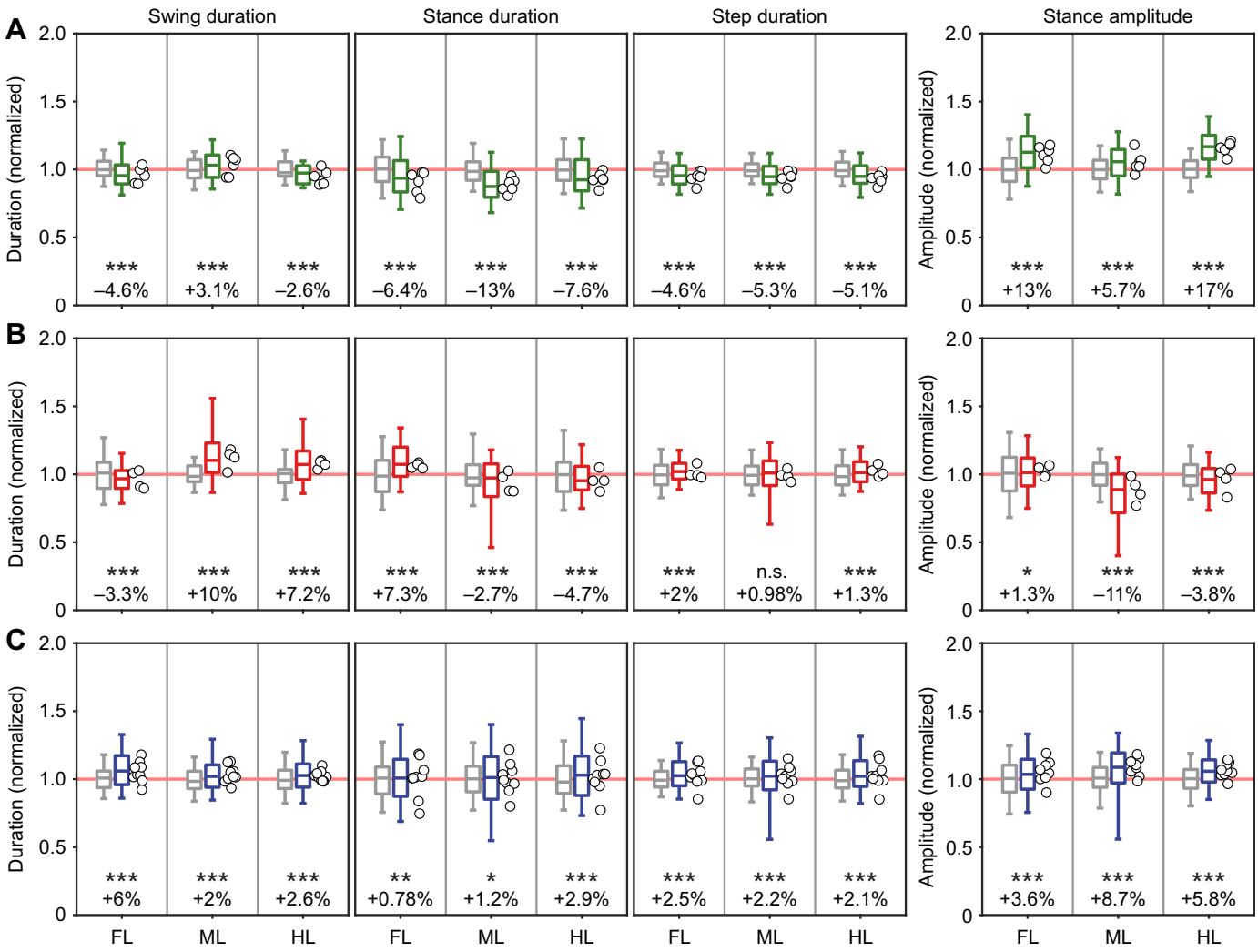

Fig. 5. Kinematic parameters of free-walking inhibition of claw, club and hook neurons. For a detailed description, see Fig. 3C legend. (A) Data for R55B03-Gal4>UAS-GtACR1 flies (green). *N*=6; *n*=872 (control) and 553 (inhibition). (B) Data for R46H11-Gal4>UAS-GtACR1 flies (red). *N*=4; *n*=368 (control) and 465 (inhibition). (C) Data for R86D09-Gal4>UAS-GtACR1 flies (blue). *N*=9; *n*=940 (control) and 1364 (inhibition).

especially when a leg experiences changes in load. In general, the differential roles of the fCO in spatial and temporal aspects of motor output during walking found in the present study also suggest that these aspects can, at least to some extent, be controlled independently in the fly's nervous system.

Transient CO inhibition produced effects similar to broader inhibition of leg sensory structures and mutations of CO-associated mechanosensitive ion channels. Using *nanchung* mutants as well as tetanus toxin-mediated silencing in leg sensory neurons (5-40-Gal4), Mendes et al. (2013) demonstrated that walking speed decreased, step length increased, stance trajectories became less linear, and AEP and PEP placement became more variable compared with that in wild-type flies. The present data show the same findings for step length, stance linearity and AEP/PEP placement, though only for the broader fCO inhibition in *iav*-Gal4 and the club/hook line. The data in the previous study (Mendes et al., 2013) indicated rather small effects with chronic silencing of nearly all leg sensory neurons (tetanus toxin light chain, TNT). The difference to the present study might lie in the contrast between transient and chronic inhibition – expressing TNT in leg sensory neurons allows much more time to compensate for a reduction in sensory information, and behavioral functionality might have been recovered to some degree in these animals. In the locust, for example, gain changes in the fCO can be recovered (Page and Matheson, 2009); this process is relatively slow, however, occurring over the span of a few days. Null mutants of *transient receptor potential-γ* (*trp-γ*), which encodes an ion channel found in mechanosensors and COs, are also impaired in fine motor control and gap crossings (Akitake et al., 2015). Moreover, flies with *nompc* mutations, which encodes a common CO TRPN channel, demonstrated increased step duration, while step amplitude was unchanged compared with that of wild-type flies (Cheng et al., 2010). The present findings add to the existing literature on the general importance of the fCO in behaviors that are reliant on leg movements; here, we extend this body of evidence and trace behavioral effects seen during walking to the acute inhibition of specific subsets of neurons within the fCO.

We cannot determine the influence of the CS labeled by R27E02-Gal4 on leg kinematics; however, because of the overlap in labeling between this driver and *iav*-Gal4, which labels no CS, as well as their similar effects on both interleg and intraleg coordination, we can assume that the population effects of the fCO neurons dominate the output. That said, it should be investigated whether the greater effects in R27E02-Gal4 on stance amplitude (Fig. 4C) compared

Journal of Experimental Biology (2022) 225, jeb244245. doi:10.1242/jeb.244245

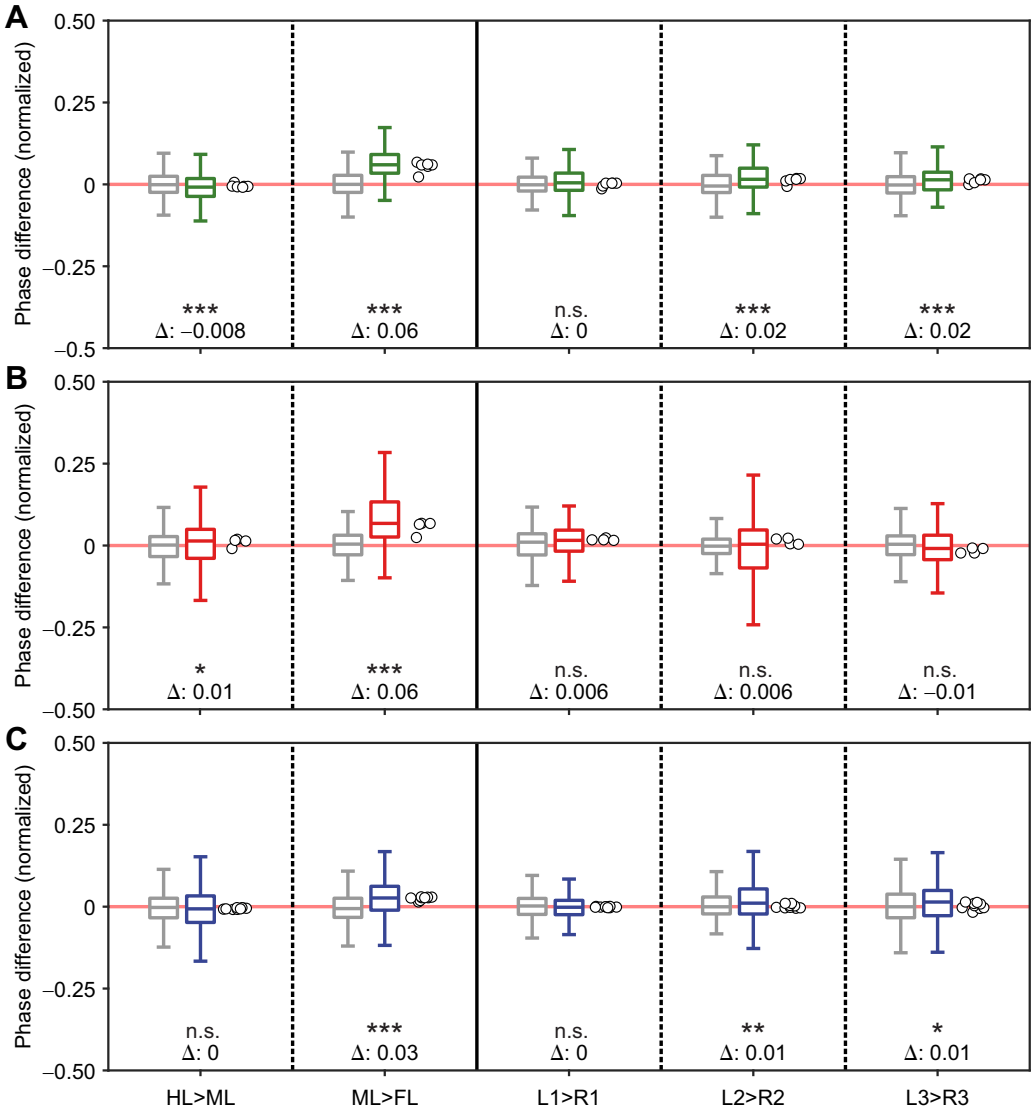

Fig. 6. Kinematic parameters of free-walking inhibition of claw, club and hook neurons. For a detailed description, see Fig. 3D legend. (A) Data for R55B03-Gal4>UAS-GtACR1 flies (green). *N*=6; *n*=436 (control) and 273 (inhibition). (B) Data for R46H11-Gal4>UAS-GtACR1 flies (red). *N*=4; *n*=184 (control) and 233 (inhibition). (C) Data for R86D09-Gal4>UAS-GtACR1 flies (blue). *N*=9; *n*=470 (control) and 681 (inhibition).

with those of *iav*-Gal4 (Fig. 3C) are due to CS influence or the interplay of multiple fCO subgroups.

Role of fCO differs for control of front, middle and hind legs

Some of the kinematic effects, mainly the swing and stance durations, seen in *iav*-Gal4 and R27E02-Gal4 differed systematically between the three leg types (front, middle, hind). The types of legs in insects differ in their involvement in certain behaviors (Cruse, 1976; Zumstein et al., 2004; Seeds et al., 2014; Dallmann et al., 2016), and in *D. melanogaster*, different kinematics are required of different legs generating the same stepping phase movements. The same movement is, thus, encoded by different proprioceptive signals and would require appropriately different post-processing.

The time in a stepping cycle that is most relevant for intraleg coordination, and which is also behaviorally well defined from a control point of view, is when to lift off (i.e. the transition from stance to swing). In the front and hind legs, this is strongly correlated with the femur–tibia joint angle. Interleg coordination, in contrast, relies more on whether neighboring legs are in swing or stance. As the signals encoded by the fCO represent only the femur–tibia joint angle and relative changes thereof, there is likely a level of abstraction upstream of this sensor.

When we inhibited a group of club/hook neurons (R27E02-Gal4), we found that swing and stance duration were affected in all legs; swing duration was highest in hind legs, while stance duration was highest in front legs (Fig. 4C). Hind leg swing and front leg stance movements both require tibial flexion. Further, one group of hook neurons has been shown to be more sensitive to tibial flexion than extension (Mamiya et al., 2018). As the neural coding of fCO neurons has only been shown for front legs, however, it is currently unknown whether the directional sensitivity of the same neurons could vary between the leg types. The results presented here certainly support a leg-specific function of otherwise identical subsets of sensory neurons.

Some club and hook neurons, but not all, are involved in leg coordination

Inhibiting most of the fCO or a subset of hook and club neurons changed stepping parameters and altered the movements of legs.

Inhibiting hook, claw or club neurons alone, however, did not have effects on the parameters tested here. This suggests that morphological categorization is not entirely congruent with putative functional categories, such as those outlined by Mamiya et al. (2018). The lack of effect on the parameters tested here could be due to a number of factors, but it could be that these neurons are simply not involved in the behavior of straight walking at moderate speed on a flat surface or are tuned to more complex leg movements, such as curve walking, gap crossing, climbing or grooming. Any behaviors involving movements of the legs – grooming, flying, etc. – should involve fCO neurons, and the importance of fCO subsets for the proper execution of these behaviors should be investigated. An alternative explanation might be a combinatorial effect of different subgroups. In that notion, any single type of neuron or subgroup alone is insufficient to have an effect on the kinematics of walking, but interaction of the afferent information provided by at least two of them would result in more pronounced changes in behavior (see also next paragraph).

The roles of these fCO subsets in walking correlate with their differential expression of presynapses in the glomerulus and within the fCO (Fig. S1). First identified by electron microscopy of the femur, the glomerulus has been suggested to be a peripheral preprocessing center for leg proprioceptive information – something never identified in other insects (Shanbhag et al., 1992; Field and Matheson, 1998). Intra-fCO connectivity, whether functional or physiological, is likely to be different between the neuron types, as seen by the synaptotagmin::GFP labeling. Only two driver lines tested here, *iav*-Gal4 and the club/hook line R27E02-Gal4, showed presynapses in the glomerulus (Fig. S1A,B); these are also the only two where inhibition affected leg kinematics. It is conceivable that sensory information important for the central control of walking behavior is preprocessed in the glomerulus, where more derived information might be calculated before it enters the CNS.

fCO inhibition mildly affects temporal coordination

Mendes et al. (2013) did not report effects on left–right or intersegmental temporal coordination, which is in accordance with our findings. The small effects on phase relationships seen here are likely due to animals walking in a well-lit arena compared with a dark arena, as control flies also showed the same effects. The phase shifts seen here seem to be caused by changes in front leg stepping; this small effect can be seen in the phase relationships between middle and front legs in control flies (Fig. S3A). It has been suggested that blow flies (*Calliphora vicina*) use their front legs as tactile probes and change the pitch of their body while walking in darkness (non-visible IR illumination; Kress and Egelhaaf, 2012); this might have been the case in the present study, but this has not been directly tested in *D. melanogaster*. The evidence we present here argues that the strongest role of the fCO during walking lies in spatial aspects of leg kinematics, and while the data show a mild effect on coordination, it is difficult to tease these two apart. That said, the lack of a strong role of the fCO subsets tested here in interleg coordination could suggest a functional segregation between temporal and spatial aspects of walking.

In summary, transient optogenetic inhibition of proprioceptor subsets in intact flies causes changes in walking kinematics, and these changes vary depending on the neurons that are silenced. Considering that fCO neurons seem to be functionally grouped based on their response profiles and anatomy (Mamiya et al., 2018), we expected a similar functional grouping regarding effects on behavioral output. Interestingly, inhibition of individual neuronal types did not affect leg kinematics (Fig. S4) but caused mild phase delays in front legs (Fig. 4). Inhibiting a group of club and hook neurons together, in contrast, affected leg kinematics similarly to inhibition of the entire fCO. This shows that fCO neuronal subsets indeed have distinct functional grouping regarding motor control, but that this grouping may not correspond to grouping based on anatomical or encoding properties. Further, peripheral presynapses are seen in the fCO itself and in a glomerulus located where fCO axons enter the leg nerve, with fCO subset driver lines displaying different patterns of presynaptic labeling in both areas (Fig. S2). Further research moving forward should test the functional relevance of leg proprioceptive signals in a wider range of behaviors in addition to the apparent fCO–fCO connectivity within and outside the glomerulus.

Acknowledgements

The authors would like to extend their appreciation for help with the conceptualization, implementation, analysis and presentation of these experiments to Dipl. Ing. Michael Dübbert, Jan Sydow, PD Dr Benjamin Altenhein, Dr Salil Bidaye, Dr Nicholas S. Szczecinski, Prof. Dr Kei Ito, Dr Jan M. Ache, Vincent Godesberg, Imiel Momoh, Carina Edel and Prof. Dr Konrad Dettner. The authors are grateful for the support of the Imaging Facility of the University of Cologne Biocenter. Parts of the text and the figures in this paper are reproduced from the doctoral dissertation of A.S.C. (Chockley, 2020).

Competing interests

The authors declare no competing or financial interests.

Author contributions

Conceptualization: A.S.C., S.R., T.B., A.B.; Methodology: A.S.C., G.F.D., T.B.; Formal analysis: A.S.C., G.F.D., G.D., T.B.; Investigation: A.S.C., G.F.D., G.D., S.R.; Data curation: A.S.C., G.F.D.; Writing - original draft: A.S.C.; Writing - review & editing: A.S.C., G.F.D., G.D., S.R., T.B., A.B.; Visualization: A.S.C., G.F.D., G.D., T.B.; Supervision: T.B., A.B.

Funding

A.S.C, G.F.D., and A.B. were supported by the Deutsche Forschungsgemeinschaft (233886668/GRK1960). G.F.D. was supported by the Deutsche Forschungsgemeinschaft (DFG DI 2907/1-1, project number 500615768). T.B. and A.B. were supported by research grant C3NS in the international NeuroNex Program (Deutsche Forschungsgemeinschaft, Bu857/15). S.R. was supported by a Fulbright Program fellowship. Open Access funding provided by Universität zu Köln. Deposited in PMC for immediate release.

References

Akay, T. (2020). Sensory feedback control of locomotor pattern generation in cats and mice. *Neuroscience* **450**, 161-167. doi:10.1016/j.neuroscience.2020.05.008

Akitake, B., Ren, Q., Boiko, N., Ni, J., Sokabe, T., Stockand, J. D., Eaton, B. A. and Montell, C. (2015). Coordination and fine motor control depend on *Drosophila* TRPγ. *Nat. Commun.* **6**, 7288. doi:10.1038/ncomms8288

Backhaus, B., Sulkowski, E. and Schlote, F. (1984). A semi-synthetic, general-purpose medium for *Drosophila melanogaster*. *Dros. Inf. Serv.* **60**, 210-212.

Bässler, U. (1965). Proprioceptoren am Subcoxal- und Femur-Tibia-Gelenk der Stabheuschrecke *Carausius morosus* und ihre Rolle bei der Wahrnehmung der Schwerkraftrichtung. *Kybernetik* **2**, 168-193. doi:10.1007/bf00272314

Bässler, U. (1967). Zur Regelung der Stellung des Femur-Tibia-Gelenkes bei der Stabheuschrecke *Carausius morosus* in der Ruhe und im Lauf. *Kybernetik* **4**, 18-26. doi:10.1007/bf00288822

Bässler, U. (1993). The femur-tibia control system of stick insects — a model system for the study of the neural basis of joint control. *Brain Res. Rev.* **18**, 207-226. doi:10.1016/0165-0173(93)90002-h

Berens, P. (2009). CircStat: a MATLAB toolbox for circular statistics. *J. Stat. Softw.* **31**, 1-21. doi:10.18637/jss.v031.i10

Burrows, M. (1996). *The Neurobiology of an Insect Brain*. Oxford: Oxford University Press.

Büschges, A. (1994). The physiology of sensory cells in the ventral scoloparium of the stick insect femoral chordotonal organ. *J. Exp. Biol.* **189**, 285-292. doi:10.1242/jeb.189.1.285

Cheng, L. E., Song, W., Looger, L. L., Jan, L. Y. and Jan, Y. N. (2010). The role of the TRP channel NompC in *Drosophila* larval and adult locomotion. *Neuron* **67**, 373-380. doi:10.1016/j.neuron.2010.07.004

Chiel, H. J., Ting, L. H., Ekeberg, O. and Hartmann, M. J. Z. (2009). The brain in its body: motor control and sensing in a biomechanical context. *J. Neurosci.* **29**, 12807-12814. doi:10.1523/jneurosci.3338-09.2009
Chockley, A. S. (2020). The role of the femoral chordotonal organ in motor control, interleg coordination, and leg kinematics in Drosophila melanogaster. Doctoral dissertation, Universität zu Köln.
Cruse, H. (1976). The function of the legs in the free walking stick insect, *Carausius morosus*. *J. Comp. Physiol.* **112**, 235-262. doi:10.1007/bf00606541
Cruse, H., Dean, J. and Suilmann, M. (1984). The contributions of diverse sense organs to the control of leg movement by a walking insect. *J. Comp. Physiol.* **154**, 695-705. doi:10.1007/bf01350223
Dallmann, C. J., Dürr, V. and Schmitz, J. (2016). Joint torques in a freely walking insect reveal distinct functions of leg joints in propulsion and posture control. *Proc. R. Soc. B Biol. Sci.* **283**, 20151708. doi:10.1098/rspb.2015.1708
Delcomyn, F. and Cocatre-Zilgien, J. H. (1988). Individual differences and variability in the timing of motor activity during walking in insects. *Biol. Cybern.* **59**, 379-384. doi:10.1007/bf00336111
Dinges, G. F., Chockley, A. S., Bockemühl, T., Ito, K., Blanke, A. and Büschges, A. (2021). Location and arrangement of campaniform sensilla in *Drosophila melanogaster*. *J. Comp. Neurol.* **529**, 905-925. doi:10.1002/cne.24987
Field, L. H. and Matheson, T. (1998). Chordotonal organs of insects. *Adv. Insect Physiol.* **27**, 1-228. doi:10.1016/s0065-2806(08)60013-2
Field, L. H. and Pflüger, H.-J. (1989). The femoral chordotonal organ: a bifunctional orthopteran (*Locusta migratoria*) sense organ? *Comp. Biochem. Physiol. Physiol.* **93**, 729-743. doi:10.1016/0300-9629(89)90494-5
Frigon, A., Akay, T. and Prilutsky, B. I. (2022). Control of mammalian locomotion by somatosensory feedback. *Compr. Physiol.* **12**, 2877-2947. doi:10.1002/cphy.c210020
Govorunova, E. G., Sineshchekov, O. A., Janz, R., Liu, X. and Spudich, J. L. (2015). Natural light-gated anion channels: A family of microbial rhodopsins for advanced optogenetics. *Science* **349**, 647-650. doi:10.1126/science.aaa7484
Hofmann, T. and Koch, U. T. (1985). Acceleration receptors in the femoral chordotonal organ of the stick insect, *Cuniculina Impigra*. *J. Exp. Biol.* **114**, 225-237. doi:10.1242/jeb.114.1.225
Hofmann, T., Koch, U. T. and Bässler, U. (1985). Physiology of the femoral chordotonal organ in the stick insect, *Cuniculina Impigra*. *J. Exp. Biol.* **114**, 207-223. doi:10.1242/jeb.114.1.207
Jenett, A., Rubin, G. M., Ngo, T.-T. B., Shepherd, D., Murphy, C., Dionne, H., Pfeiffer, B. D., Cavallaro, A., Hall, D., Jeter, J. et al. (2012). A GAL4-driver line resource for *Drosophila* neurobiology. *Cell Rep.* **2**, 991-1001. doi:10.1016/j.celrep.2012.09.011
Kondoh, Y., Okuma, J., Newland, P. L. (1995). Dynamics of neurons controlling movements of a locust hind leg: Wiener kernel analysis of the responses of proprioceptive afferents. *J. Neurophysiol.* **73**, 1829-1842. doi:10.1152/jn.1995.73.5.1829
Kress, D. and Egelhaaf, M. (2012). Head and body stabilization in blowflies walking on differently structured substrates. *J. Exp. Biol.* **215**, 1523-1532. doi:10.1242/jeb.066910
Mamiya, A., Gurung, P. and Tuthill, J. C. (2018). Neural coding of leg proprioception in *Drosophila*. *Neuron* **100**, 636-650.e6. doi:10.1016/j.neuron.2018.09.009
Matheson, T. (1992). Morphology of the central projections of physiologically characterised neurones from the locust metathoracic femoral chordotonal organ. *J. Comp. Physiol.* **170**, 101-120. doi:10.1007/bf00190405
Mathis, A., Mamidanna, P., Cury, K. M., Abe, T., Murthy, V. N., Mathis, M. W. and Bethge, M. (2018). DeepLabCut: markerless pose estimation of user-defined body parts with deep learning. *Nat. Neurosci.* **21**, 1281-1289. doi:10.1038/s41593-018-0209-y
Mendes, C. S., Bartos, I., Akay, T., Márka, S. and Mann, R. S. (2013). Quantification of gait parameters in freely walking wild type and sensory deprived *Drosophila melanogaster*. *Elife* **2**, e00231. doi:10.7554/elife.00231
Mendes, C. S., Rajendren, S. V., Bartos, I., Márka, S. and Mann, R. S. (2014). Kinematic responses to changes in walking orientation and gravitational load in *Drosophila melanogaster*. *PLoS One* **9**, e109204. doi:10.1371/journal.pone.0109204
Mohammad, F., Stewart, J. C., Ott, S., Chlebikova, K., Chua, J. Y., Koh, T.-W., Ho, J. and Claridge-Chang, A. (2017). Optogenetic inhibition of behavior with anion channelrhodopsins. *Nat. Methods* **14**, 271-274. doi:10.1038/nmeth.4148
Page, K. L. and Matheson, T. (2009). Functional recovery of aimed scratching movements after a graded proprioceptive manipulation. *J. Neurosci.* **29**, 3897-3907. doi:10.1523/jneurosci.0089-09.2009
Pearson, K. G. (1995). Proprioceptive regulation of locomotion. *Curr. Opin. Neurobiol.* **5**, 786-791. doi:10.1016/0959-4388(95)80107-3
Phillis, R., Statton, D., Caruccio, P. and Murphey, R. K. (1996). Mutations in the 8 kDa dynein light chain gene disrupt sensory axon projections in the Drosophila imaginal CNS. *Development* **122**, 2955-2963. doi:10.1242/dev.122.10.2955
Schindelin, J., Arganda-Carreras, I., Frise, E., Kaynig, V., Longair, M., Pietzsch, T., Preibisch, S., Rueden, C., Saalfeld, S., Schmid, B. et al. (2012). Fiji: an open-source platform for biological-image analysis. *Nat. Methods* **9**, 676-682. doi:10.1038/nmeth.2019
Seeds, A. M., Ravbar, P., Chung, P., Hampel, S., Midgley, F. M., Mensh, B. D. and Simpson, J. H. (2014). A suppression hierarchy among competing motor programs drives sequential grooming in *Drosophila*. *Elife* **3**, e02951. doi:10.7554/elife.02951
Shanbhag, S. R., Singh, K. and Singh, R. N. (1992). Ultrastructure of the femoral chordotonal organs and their novel synaptic organization in the legs of *Drosophila melanogaster* Meigen (Diptera: Drosophilidae). *Int. J. Insect Morphol. Embryol.* **21**, 311-322. doi:10.1016/0020-7322(92)90026-j
Simon, J. C. and Dickinson, M. H. (2010). A new chamber for studying the behavior of *Drosophila*. *PLoS One* **5**, e8793. doi:10.1371/journal.pone.0008793
Stein, W. and Sauer, A. E. (1999). Physiology of vibration-sensitive afferents in the femoral chordotonal organ of the stick insect. *J. Comp. Physiol.* **184**, 253-263. doi:10.1007/s003590050323
Strauß, J. (2017). The scolopidial accessory organs and Nebenorgans in orthopteroid insects: comparative neuroanatomy, mechanosensory function, and evolutionary origin. *Arthropod. Struct. Dev.* **46**, 765-776. doi:10.1016/j.asd.2017.08.004
Strauß, R. and Heisenberg, M. (1990). Coordination of legs during straight walking and turning in Drosophila melanogaster. *J. Comp. Physiol.* **167**, 403-412. doi:10.1007/bf00192575
Tsubouchi, A., Yano, T., Yokoyama, T. K., Murtin, C., Otsuna, H. and Ito, K. (2017). Topological and modality-specific representation of somatosensory information in the fly brain. *Science* **358**, 615-623. doi:10.1126/science.aan4428
Tuthill, J. C. and Azim, E. (2018). Proprioception. *Curr. Biol.* **28**, R194-R203. doi:10.1016/j.cub.2018.01.064
Tuthill, J. C. and Wilson, R. I. (2016). Mechanosensation and adaptive motor control in insects. *Curr. Biol.* **26**, R1022-R1038. doi:10.1016/j.cub.2016.06.070
Usherwood, P. N. R., Runion, H. I. and Campbell, J. I. (1968). Structure and physiology of a chordotonal organ in the locust leg. *J. Exp. Biol.* **48**, 305-323. doi:10.1242/jeb.48.2.305
Weiland, G. and Koch, U. T. (1987). Sensory feedback during active movements of stick insects. *J. Exp. Biol.* **133**, 137-156. doi:10.1242/jeb.133.1.137
Weiland, G., Bässler, U. and Brunner, M. (1986). A biological feedback control system with electronic input: the artificially closed femur-tibia control system of stick insects. *J. Exp. Biol.* **120**, 369-385. doi:10.1242/jeb.120.1.369
Wosnitza, A., Bockemühl, T., Dübbert, M., Scholz, H. and Büschges, A. (2013). Inter-leg coordination in the control of walking speed in Drosophila. *J. Exp. Biol.* **216**, 480-491. doi:10.1242/jeb.078139
Zill, S. N. (1987). Selective mechanical stimulation of an identified proprioceptor in freely moving locusts: role of resistance reflexes in active posture. *Brain Res.* **417**, 195-198. doi:10.1016/0006-8993(87)90200-9
Zumstein, N., Forman, O., Nongthomba, U., Sparrow, J. C. and Elliott, C. J. H. (2004). Distance and force production during jumping in wild-type and mutant *Drosophila melanogaster*. *J. Exp. Biol.* **207**, 3515-3522. doi:10.1242/jeb.01181

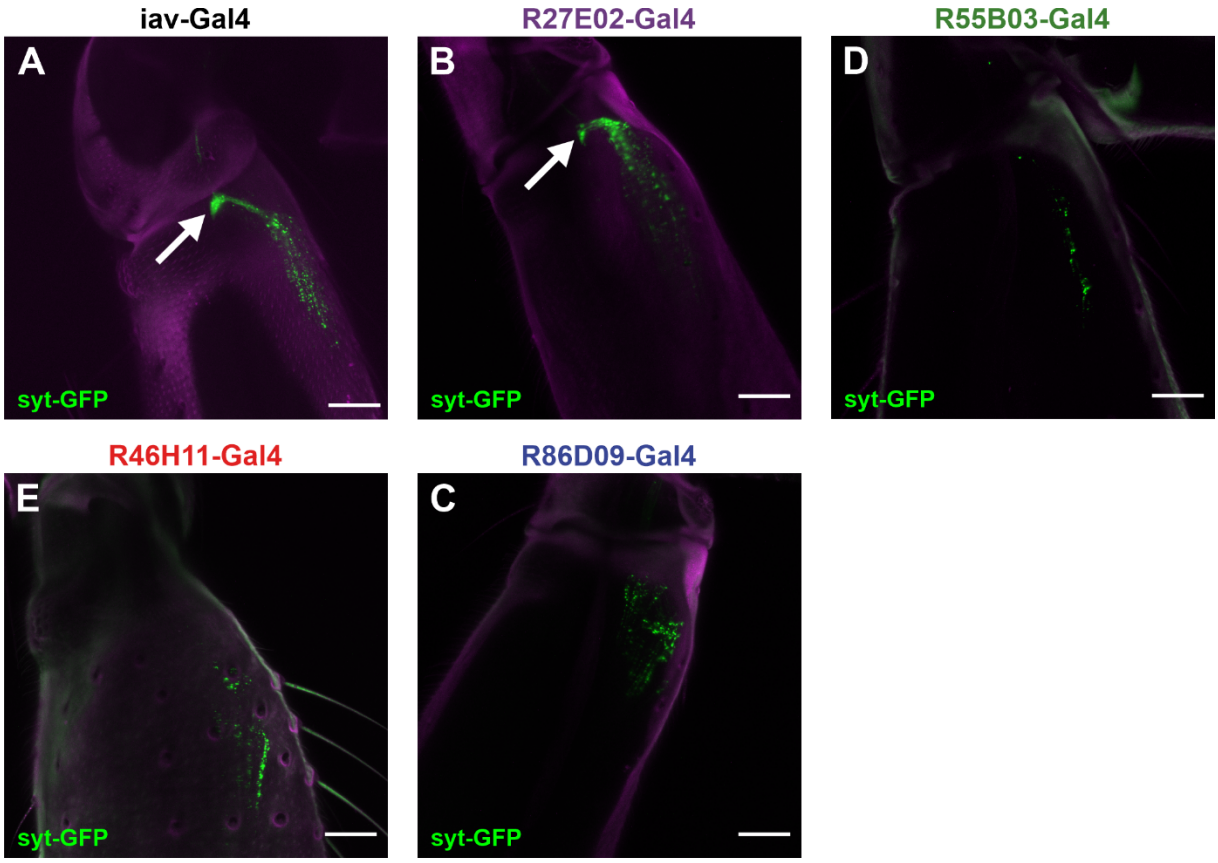

Fig. S1. Syt-GFP labeling of fCO Gal4 driver lines. Gal4-controlled expression of syt-GFP (green) shows presynapses of the glomerulus in iav-Gal4 (A, white arrow) and R27E02-Gal4 (B, white arrow) as well as intra-fCO presynapses in all lines (A-E). Magenta is cuticular autofluorescence for orientation. Scale bars: 25 µm.

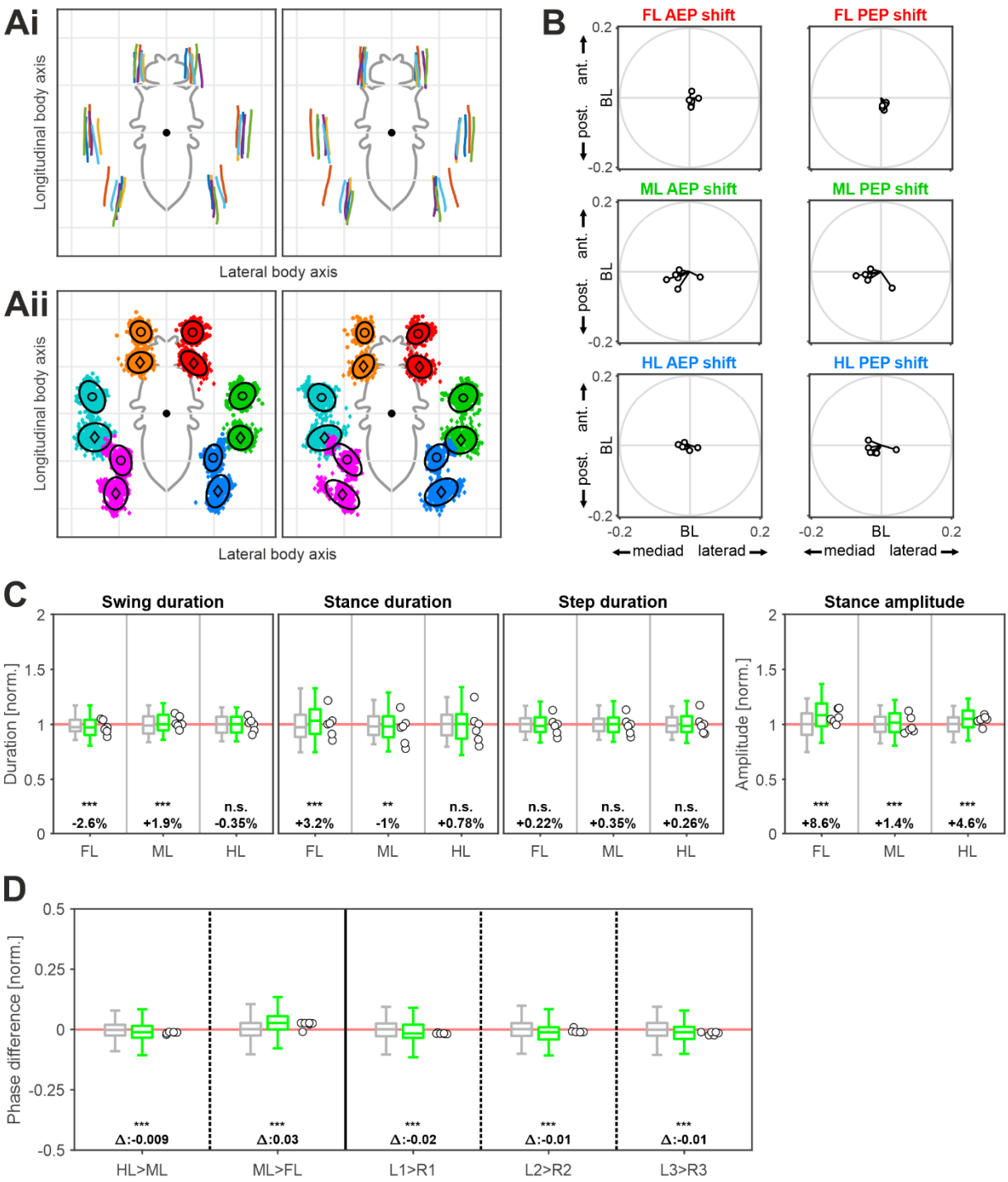

Fig. S2. Kinematic parameters and temporal coordination of free walking in control Berlin-K>UAS-GtACR flies. For detailed description see legend of Fig. 3. (A) Number of individual flies (N) is 6 in Ai, each fly is a different color. The minimum number of steps (n) per leg in Aii is 540 (dark, left) and 528 (green light, right). (B) N = 6. (C) N = 6. The minimum number of steps (n) per leg in panel C is 1046 (dark, gray) and 1023 (green light, green box plots), respectively. (D) The minimum number of steps (n) per leg in panel D is 521 (dark) and 509 (green light), respectively. (B and D) The color associated with inhibition data has been set to bright green (wildtype Berlin-K>UAS-GtACR1, no expression of Gal4 or GtACR1).

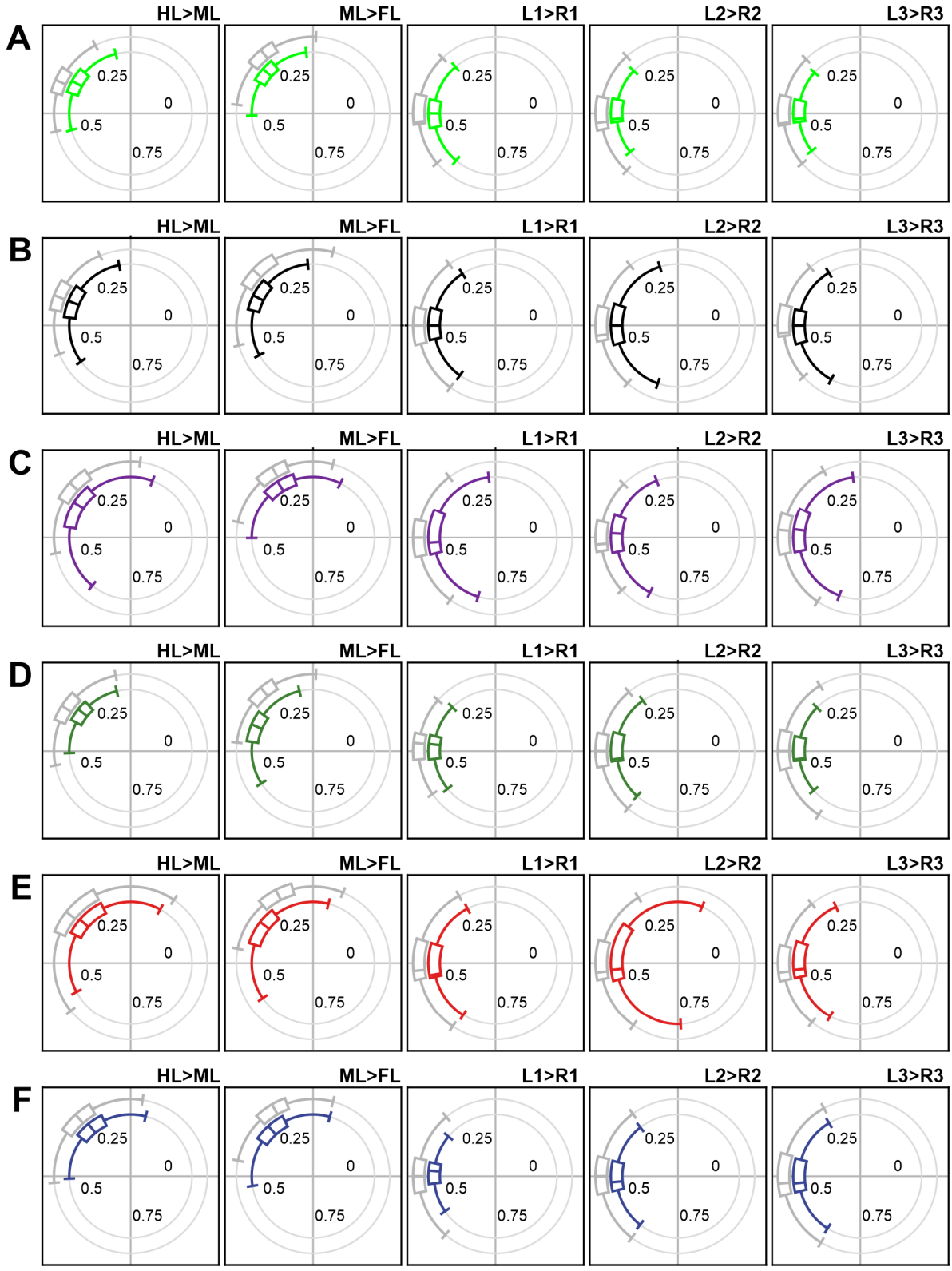

Fig. S3. Absolute phase relationships between adjacent legs. Each row depicts phase data as circular boxplots. Data for each line has been pooled. Outer boxplots (gray) depict interleg coordination in darkness (control), inner boxplots depict phase relationships during green light (inhibition). (A) Data for Berlin-K>UAS-GtACR1 flies.

N = 6, minimum number of steps (n) per leg in 521 (dark) and 509 (green light), respectively. (B) Data for Iav-Gal4>UAS-GtACR1 flies. N = 5, minimum number of steps (n) per leg is 374 (control) and 226 (inhibition), respectively. (C) Data for R27E02-Gal4>UAS-GtACR1 flies. N = 7, minimum number of steps (n) per leg is 521 (control) and 509 (inhibition), respectively. (D) Data for R55B03-Gal4>UAS-GtACR1 flies. N = 6, minimum number of steps (n) per leg is 436 (control) and 273 (inhibition), respectively. (E) Data for R46H11-Gal4>UAS-GtACR1 flies. N = 4, minimum number of steps (n) per leg is 184 (control) and 233 (inhibition), respectively. (F) Data for R86D09-Gal4>UAS-GtACR1 flies. N = 9, minimum number of steps (n) per leg is 470 (control) and 681 (inhibition), respectively.

Table S1. Reagents and Experimental Model Organism Details

REAGENT or RESOURCE	SOURCE	IDENTIFIER
Antibodies		
mouse anti-Bruchpilot (anti-nc82)	DSHB	RRID:AB_2314866
Mouse anti-ChAT4B1	DSHB	RRID:AB_528122
Rabbit anti-GFP	Invitrogen	RRID:AB_221569
Goat anti-mouse AlexaFluor 633	ThermoFisher Scientific	RRID:AB_1307538
Goat anti-rabbit AlexaFluor 488	Molecular Probes	RRID:AB_143165
Chemicals, Peptides, and Recombinant Proteins		
SigmaCote	Sigma-Aldrich	Cat #SL2
Vectashield	Vector Laboratories	RRID:AB_2336789
Normal Goat Serum	ThermoFisher Scientific	RRID:AB_2532166
Normal Donkey Serum	Jackson ImmunoResearch	RRID AB_2337258
DAPI	Carl Roth	Cat #6335.1
Experimental Models: Organisms/Strains		
Drosophila: w^{1118}; +/+; P{GMR86D09-GAL4}attP2	BDSC	RRID:BDSC_40459
Drosophila: w^{1118}; +/+; P{GMR27E02-GAL4}attP2	BDSC	RRID:BDSC_49222
Drosophila: w^{1118}; +/+; P{GMR46H11-GAL4}attP2	BDSC	RRID:BDSC_50284
Drosophila: w^{*}; +/+; P{iav-GAL4.K}3	BDSC	RRID:BDSC_52273
Drosophila: y^{1} w^{*} P{10XUAS-IVS-mCD8::GFP}su(Hw)attP8	BDSC	RRID:BDSC_32189
Drosophila: w^{*}; P{UAS-syt.eGFP}3	BDSC	RRID:BDSC_6926
Drosophila: w^{1118}; P{$y^{+t7.7}$ w^{+mC} GMR55B03-GAL4}attP2	BDSC	RRID:BDSC_39101
Drosophila: Berlin-K	BDSC	RRID:BDSC_8522
Drosophila: w^{1118}; +/+; P{20x-UAS-GtACR1-EYFP}attp2, Sb^{1}	Adam Claridge-Chang	N/A
Drosophila: P{w^{+mc}=UAS-RedStinger}3, w^{1118}	BDSC	RRID:BDSC_8545

DSHB, Developmental Studies Hybridoma Bank, IA, USA; BDSC, Bloomington Drosophila Stock Center, IN, USA